Journal of Marine Science and Technology, Vol. 24, No. 6, pp. 1129-1135 (2016)
DOI: 10.6119/JMST-016-1026-1

CAPABILITY OF GEOSTATIONARY SATELLITE IMAGERY FOR SEA ICE MONITORING IN THE BOHAI AND YELLOW SEAS

Hwa-Seon Lee and Kyu-Sung Lee

Key words: sea ice monitoring, geostationary satellite, GOCI, temporal resolution, sea ice detection, spatial filtering.

ABSTRACT

On a regional scale, sea ice monitoring is important for marine transportation, fishery, harbor and offshore structures, and weather forecast. In this study, we attempt to analyze the potential of Geostationary Ocean Color Imager (GOCI) images for regional-scale sea ice monitoring. GOCI images obtained from December 2011 to March 2012 were analyzed to evaluate the frequency that sea ice can be observed in the Bohai Sea and the northern Yellow Sea. In this season, the sea ice distribution varies greatly both temporally and spatially. During the approximate 100-day ice period, GOCI provided relatively cloud-free daily images over sea ice 86% in Liaodong Bay and 81% in Seohan Bay. In addition, GOCI was able to provide all eight hourly images from morning to late afternoon with clear condition, which is important for tracking ice drift, for 40 days in Liaodong Bay and 31 days in Seohan Bay. The high temporal resolution of GOCI facilitates short-period monitoring and tracking of sea ice. We also proposed a simple method to detect and delineate the sea ice area (SIA) from the GOCI images. A simple standard deviation filtering enhanced the spatial variability between the sea ice and open water and was very effective in separating SIA from sea water.

I. INTRODUCTION

Sea ice has many important roles ranging from global climate change to local marine transportation. On a regional scale, the distribution of sea ice is a critical factor in the heat balance because of the large albedo difference between open water and ice, and hence the strong impact on regional weather systems (Tschudi et al., 2008). In addition, sea ice restricts ship traffic during the winter season, which causes severe economic losses in the fishery and transportation industries, and often severely damages harbor facilities and offshore structures for petroleum operations (Liu et al., 2000).

Aerial survey and ground stations were the standard observation tools until satellite remote sensing became the primary operational practice for sea ice monitoring. By providing continuous synoptic views, remote sensing imagery from satellites has been effectively used to monitor the extent and distribution of sea ice over large geographic areas. Most sea ice occurs in polar and high latitude regions that have relatively short daytime for several months and are frequently cloud covered. Hence, optical images cannot be used to observe sea ice and sea ice monitoring has primarily relied on passive microwave sensor and synthetic aperture radar (SAR) imagery. Although passive microwave sensor imagery has been a major source of information on sea ice area and thickness, it may not be suitable for monitoring relatively small sea areas because of its coarse spatial resolution in the range of tens of kilometers (Drüe and Heinemann, 2004). The high spatial resolution of SAR imagery has become a major data source for operational sea ice monitoring in several countries, including Canada (Scheuchl et al., 2004). However, satellite SAR images may not have sufficient temporal resolution to derive daily and hourly sea ice information. The temporal resolution of satellite imagery is an important matter, in particular to track sea ice drift for the area of highly variable sea motion (Lang et al., 2014).

Optical remote sensor imagery is still very effective for observing sea ice under cloud-free conditions. The most common optical sensors used for sea ice are the Advanced Very High Resolution Radiometer (AVHRR) and the Moderate Resolution Imaging Spectroradiometer (MODIS), which provide spatial resolution of 0.5-1 km and daily observation capability. From these images, spectral reflectance or albedo in the visible and near-infrared (NIR) wavelengths has been used to classify sea ice type and to estimate ice thickness (Tschudi et al., 2008; Ning et al., 2009; Shi and Wang, 2012a).

In this study, we attempt to analyze the potential of Geostationary Ocean Color Imager (GOCI) imagery for regional sea ice monitoring. Unlike polar orbit satellites, GOCI can provide eight daytime images per day and therefore greatly enhance the temporal resolution of sea ice observation, to an hourly extent,

Paper submitted 05/27/16; revised 10/06/16; accepted 10/14/16. Author for correspondence: Kyu-Sung Lee (e-mail: ksung@inha.ac.kr).
Department of Geoinformatic Engineering, Inha University, Incheon, Republic of Korea.

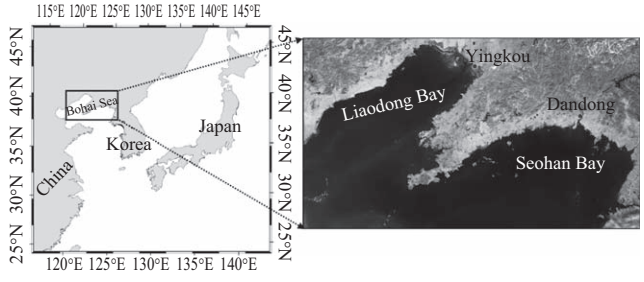

Fig. 1. Geographical coverage of the Geostationary Ocean Color Imager (GOCI) target area (approximately 2,500 × 2,500 km^2) in northeast Asia, and the two bays (Liaodong and Seohan) selected for this study.

and increase the frequency of obtaining cloud-free images. During the winter season of 2011-2012, SIA data were extracted and analyzed for the study area in the Bohai Sea and the northern Yellow Sea.

II. STUDY AREA AND DATA USED

GOCI is a suite of major imaging sensors onboard the Communication Ocean and Meteorological Satellite (COMS), which was launched on June 27, 2010 to a geostationary orbit of 36,000 km altitude. GOCI is indeed unique and perhaps the first ocean color sensor to provide continuous images on a regional scale, which covers an area of about 2,500 × 2,500 km^2 centered at 130°E × 36°N (Kang et al., 2010; Ryu et al., 2012). The GOCI images have a 500 m spatial resolution and provide eight hourly observations during daytime. As the name implies, GOCI was mainly designed for ocean color monitoring with eight spectral bands of visible and NIR wavelengths. The GOCI target area covers the northeast Asian region, including all of the Korean peninsula, Japan and part of China, Mongolia, and Russia. Fig. 1 shows the coverage of the GOCI target area and the study area of Liaodong and Seohan Bays.

The Bohai and Yellow Seas, located between the Korean peninsula and the eastern coast of China, are the southernmost latitudinal area for seasonal sea ice formation in the world. Because of high population density and rapid industrialization, this area has become very important for economic growth, with strong consequent impacts on the regional environment and weather system. Sea ice in the Bohai and Yellow Seas has caused serious problems in marine transportation, fishery, and offshore petroleum operation (Liu et al., 2000; Yang, 2000). High temporal resolution of sea ice observation is essential to reduce hazards in harbor facilities and offshore structures like oil rigs (Yue et al., 2008). In recent years, sea ice in the Bohai Sea has been studied to solve the problem of serious freshwater shortage in the surrounding region (Yuan et al., 2012). The spatial and temporal variations of sea ice in this region both affect and are affected by the regional climate system (Shi and Wang, 2012b).

Siberia high pressure controls air temperature and wind direction over this area during winter (Yang, 2000). The continental high pressure provides relatively clear sky when a cold air mass is moving over the region, which enables sea ice observation by optical remote sensor data. Several studies have used optical satellite images to examine sea ice in the Bohai Sea. MODIS data have been frequently used to estimate sea ice thickness (Ning et al., 2009; Shi and Wang, 2012b) while AVHRR data have been used to quantify the volume of sea ice for freshwater resource (Yuan et al., 2012). Since most sea ice in the Bohai Sea is floating, the monitoring of ice drift is also very important. Lang et al. (2014) has demonstrated the effectiveness of GOCI hourly images for tracking sea ice drift in the Bohai Sea.

For this study, we used GOCI images obtained during the winter season from December 2011 to March 2012. The Korea Institute of Ocean Science and Technology (KIOST) has provided GOCI images since April 2011 (Ryu et al., 2012). Early calibration works showed that the radiometric quality of GOCI radiance values is comparable with that of other polar orbit satellite data for ocean and land observations (Lamquin et al., 2012; Lee et al., 2012). KIOST supplies GOCI data at several processing levels, in which level 1B is radiometrically calibrated and geometrically corrected at-sensor radiance. GOCI level 2 products are mostly related to ocean information, such as atmospherically corrected remote sensing reflectance (RSr), water-leaving radiance, chlorophyll content, and total suspended sediment. Initially, we tried to use the RSr hourly product. However, the GOCI RSr product was not suitable for this study because most of SIA was masked out in the cloud masking process during the atmospheric correction. Instead, we used the GOCI reflectance data after normalization of downward solar irradiance variation and correction of Rayleigh scattering.

Every GOCI hourly image from December 1, 2011 to March 15, 2012 was obtained and the subset study area was extracted. To compare the temporal resolution and the SIA distribution extracted from GOCI images, we used MODIS Aqua surface reflectance (MYD09) product and sea ice product (MYD29) acquired during the same 2011-2012 winter season. Once these data were downloaded, they were mosaicked and geometrically registered to the GOCI images. Air temperature and precipitation data were obtained from two ground weather stations (Yingkou and Dandong) nearby Liaodong and Seohan Bays. Fig. 2 shows the daily minimum and maximum air temperatures at the two weather stations. Although the surface air temperature over the sea might be colder than that of ground, the minimum temperature recorded at the two nearby weather stations was below minus 20 degree in Celsius for the coldest day during the winter.

III. EVALUATION OF GOCI TEMPORAL RESOLUTION FOR SEA ICE OBSERVATION

Geostationary satellites provide higher temporal resolution than polar orbit satellites and have already demonstrated it in the derivation of cloud-free time series observations on land surfaces. The Spinning Enhanced Visible and InfraRed Imager (SEVIRI) data from the European geostationary satellite have clearly showed their effectiveness in producing

Table 1. Classification of cloudiness over sea ice.

Cloudiness class	Definition
Clear	Cloud free, 25% or less cloud cover over sea ice
Thin cloudy	Thin but transparent cloud, 25% or less cloud cover over sea ice
Partly cloudy	25%~75% cloud cover over sea ice
Cloudy	More than 75% cloud cover over sea ice

Table 2. Number of GOCI hourly images by cloudiness class in Liaodong and Seohan Bays during the sea ice period.

Ice period / Cloudiness	Liaodong Bay	Seohan Bay
	106 days (Dec. 1, 2011 ~ Mar. 15, 2012)	80 days (Dec. 5, 2011 ~ Mar. 3, 2012)
Clear	454 (53.9%)	351(55.3%)
Thin cloudy	141 (16.7%)	52 (8.2%)
Partly cloudy	70 (8.3%)	65 (10.2%)
Cloudy	177 (21.0%)	167 (26.3%)
total	842	635

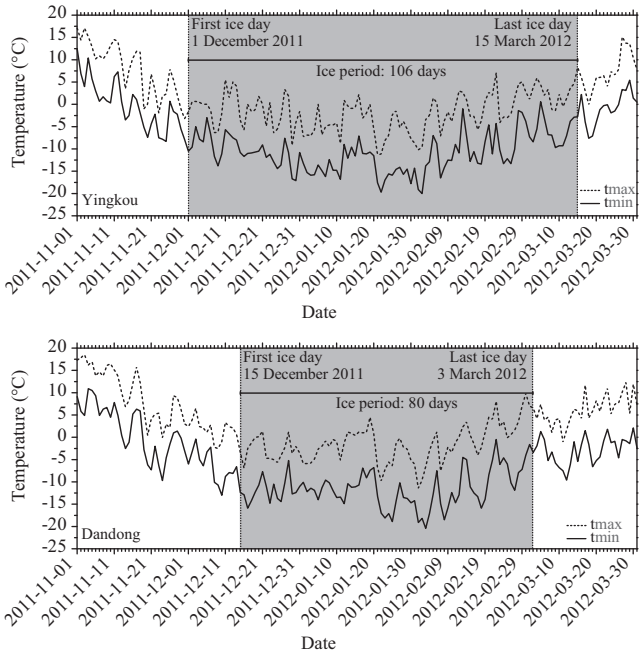

Fig. 2. Daily minimum and maximum air temperatures collected at two weather stations (Yingkou and Dandong) nearby Liaodong and Seohan Bays during the ice period from December 2011 to March 2012.

cloud-free vegetation index (VI) data with much shorter composite period compared to polar orbit satellite data over Africa (Fensholt et al., 2007). GOCI is the first regional-scale geostationary satellite sensor capable of capturing images with comparable spatial resolution and temporal resolution over the northeast Asian region. In this study, we evaluated the efficiency of this rare case of geostationary satellite images in observing sea ice.

To evaluate the potential of using the high temporal resolution of GOCI data for sea ice monitoring, all the hourly GOCI images obtained over the study area during the winter were visually interpreted to assess cloud coverage over sea ice in the two bays. In Liaodong and Seohan Bays, the sea ice period was 106 and 80 days, and 842 and 635 hourly images obtained during the sea ice period were interpreted, respectively.

The extent of cloudiness over sea ice was classified into four classes that approximated the cloudiness definition by the World Meteorological Organization (Table 1). Four cloudiness classes were visually interpreted on the RGB color images composited by NIR, red, and green wavelength bands. Sea ice has distinct spatial and tonal characteristics that are separable from open water and are easily identifiable by visual interpretation. Snow-covered sea ice and cloud have similar spectral characteristics, which renders their differentiation difficult. Sea ice in Liaodong and Seohan Bays only occurs seasonally from December to March and has apparent spatial variation during winter. Sea ice formation in this area begins from the coast in December and expands to the center of the bay as the air temperature drops. SIA declines as the air temperature begins to rise in late February. Using the temporal and spatial pattern of SIA, we were able to delineate approximate ice edges even if they were partially cloud-covered. If the cloudiness class was either 'clear' or 'thin cloudy', SIA could be easily interpreted.

Visual interpretation on every hourly GOCI image was conducted sequentially from early December to late March in order to trace SIA without significant misinterpretation. As seen in Table 2, 70.6% of 842 hourly images could be used to observe sea ice with less than 25% cloud coverage in Liaodong Bay. The frequency of relatively clear condition (clear or thin cloudy) was decreased to 63.5% in Seohan Bay where the sea ice period is shorter than in Liaodong Bay. In either case, GOCI provided many clear images that were suitable for observing and monitoring sea ice in two bays during the winter.

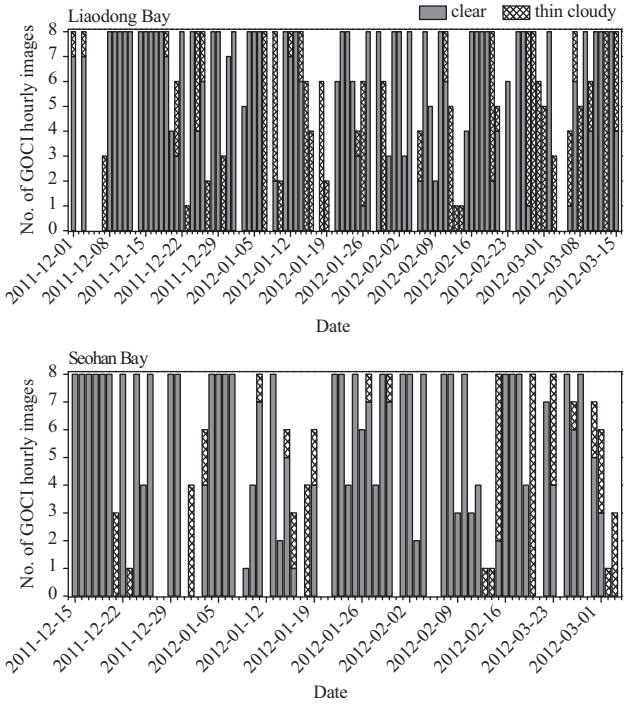

Fig. 3. Number of GOCI hourly images with relatively clear condition obtained each day during the sea ice period in the two bays.

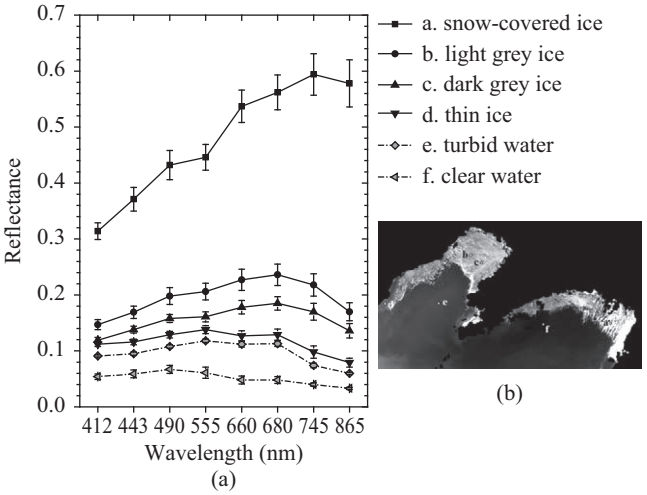

Fig. 4. Spectral reflectance of sea ice and water classes (a) that were extracted from several sites on the color composite of the GOCI images obtained in clear sky condition. The GOCI image (b), of February 4, 2012, showed typical sites of each ice and water classes sampled.

Fig. 3 shows the number of relatively clear images for each day during the winter. At least one relatively clear image was available for 91 days in Liaodong Bay and for 65 days in Seohan Bay. This high temporal resolution of the GOCI imagery for sea ice observation can be beneficial in the Bohai and Yellow Seas where SIA and drift are highly variable. Although there were two and three heavy cloudy cases lasting more than two consecutive days in Liaodong and Seohan Bays, respectively, GOCI provided 86% and 81% chance for daily sea ice observation during the ice period. The high temporal resolution of GOCI was more evident in comparison with the polar orbit satellite images of MODIS. The MODIS images obtained during the same ice period were also categorized into four cloudiness classes by the equal visual interpretation criterion applied to the GOCI images. MODIS provided 77 and 50 days of clear or thin cloudy images in Liaodong and Seohan Bays, respectively, which was about 16% less than GOCI.

As reported by Lang et al. (2014), the tracking of sea ice drift in the Bohai Sea is very important to reduce the damage to offshore structures. They have already demonstrated the capability of GOCI hourly images to be used to track sea ice drift on an hourly basis. During the sea ice period, GOCI was able to provide clear condition images for all eight hourly observations for 40 days in Liaodong Bay and for 31 days in Seohan Bay. If we apply rather loose cloudiness condition, four or more relatively clear (clear or thin cloudy) hourly images were obtained for 77 days in Liaodong Bay and 52 days in Seohan Bay. Although MODIS might provide many cloud-free daily images (only 16% less than GOCI), it could not deliver images for tracking sea ice drift. Sea ice in this area is a seasonal phenomenon with a maximum thickness of less than 1 m and, therefore, its formation is highly variable spatially and temporally due to sea current, wind speed and direction, and surface air temperature. GOCI is the first satellite imagery capable of short-period tracking of sea ice drift over this highly variable sea area.

IV. SEA ICE DETECTION ON GOCI IMAGES

It would be straightforward to detect sea ice from open water if the spectral reflectance of sea ice, which is higher than that of water in visible and NIR wavelengths, is homogenous. However, the spectral reflectance of sea ice varies greatly according to the surface conditions, ice bubbles, and ice thickness (Grenfell and Perovich, 1984; Riggs et al., 1999; Perovich et al., 2002). Furthermore, the spectral reflectance of sea ice in the Bohai and Yellow Seas is very sensitive to the impurity content within ice, which is often difficult to separate from the highly turbid sea water (Ning et al., 2009). Most sea ice detection algorithms on optical remote sensor imagery are based on a grouped-criteria threshold on band reflectance, band ratio, or normalized difference snow index (NDSI) (Hall et al., 1995; Shi and Wang, 2012b). However, as Shi and Wang (2012b) showed, the MODIS sea ice product algorithm, which is also based on NDSI and band reflectance threshold, fails to detect sea ice in the Bohai Sea because of the complex optical property of ice and turbid water in this region.

Before attempting to separate sea ice from open water, we tried to compare the spectral reflectance of sea ice and open sea water in GOCI wavelength bands. From the color composite of cloud-free GOCI images, we selected several sites of different ice and water types and extracted reflectance values from about twenty sites for each class (Fig. 4(b)). The sea ice

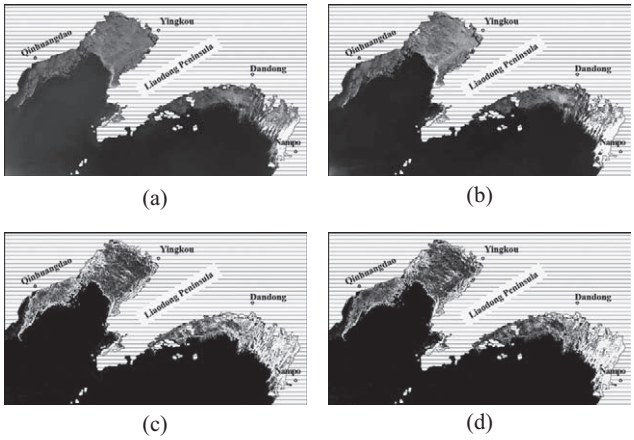

Fig. 5. GOCI images of the green (a) and NIR bands (b) obtained on February 4, 2012. These two images were filtered by a 3 × 3 standard deviation filter and the outputs are (c) and (d), respectively.

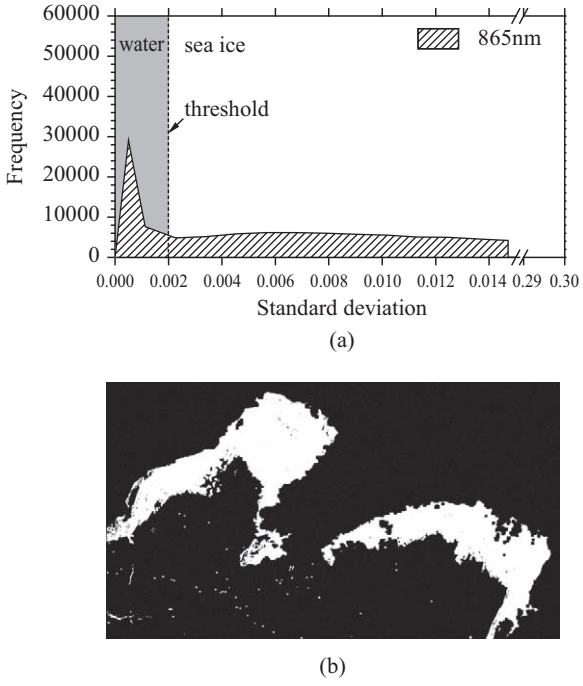

Fig. 6. Histogram of the output NIR image after applying a 3 × 3 standard deviation filter on the NIR band (a) and the extracted sea ice area (SIA) by the threshold on the histogram (b).

and water types were mainly identified by the visual interpretation of GOCI color images, whereas the snow-covered sea ice was confirmed by the precipitation data obtained nearby weather stations. Fig. 4(a) shows the reflectance values at eight GOCI bands from visible and NIR wavelengths for snow-covered ice, light grey ice, dark grey ice, thin ice, turbid water, and clear water. The four sea ice classes have higher reflectance than sea water and could be separated from clear sea water. However, thin ice near the edge and turbid water are spectrally similar and could not be separated well with these spectral bands.

Considering the spectral similarity between thin ice and turbid water, a threshold on GOCI band reflectance may not be effective for separating thin ice area. We proposed a simple method that uses the spatial variability of sea ice surface. The reflectance values of sea ice shows high spatial variability within a distance of a few kilometers. The surface condition of sea ice changes quickly within a small spatial domain by roughness, snow, hummock, and thickness. Spatial convolution filtering was applied in which the center pixel within the window was substituted by the standard deviation of all the pixels within the window. Standard deviation filter is normally used to measure the image texture and to enhance the edge between two different cover types. Standard deviation of sea ice within a window was expected to be much higher than that of open water. Sea water is relatively homogeneous within a short distance and its standard deviation within a window is much lower than that of sea ice.

We applied a 3 × 3 standard deviation filter on the green (555 nm) and NIR (865 nm) band images after excluding the land area (Fig. 5). The highly turbid water, as seen in the green band image (Fig. 5(a)), is prominent on the lower left side of the image. The boundary between the thin sea ice edge and turbid water is not very clear (near the coast of south Qinhuangdao) because of the mixed spectral characteristics. Both clear and turbid waters have low reflectance and look very dark in the NIR band image (Fig. 5(b)), which is relatively homogenous compared to SIA. Although the reflectance images of the green and NIR bands are rather different in the open water area because of the turbidity, the filtered outputs are almost identical (Figs. 5(c) and 5(d)). After applying a 3 × 3 standard deviation filter, the two output images demonstrated the effectiveness for detecting ice edges that are apparent even from the turbid water. Although the two filtered images look almost identical, the NIR band image that has low spatial variability within sea water is a better choice to separate sea ice from water. SIA was extracted from the filtered NIR band image. In the histogram (Fig. 6(a)) of the filtered NIR image (Fig. 5(d)), a threshold between sea ice and open water can be easily determined. Applying the threshold obtained from the filtered NIR image, the exact SIA was extracted (Fig. 6(b)).

Using the proposed method of detecting sea ice, all the GOCI daily images obtained in clear condition were processed to extract SIA during the ice period in Liaodong and Seohan Bays. Fig. 7(a) shows the temporal changes of SIA extracted from the GOCI images during the winter. SIA was largest in early February in both bays. After then, SIA declined quickly and disappeared in March. In Seohan Bay, where the sea ice period is shorter, all the sea ice melted in early March, whereas the sea ice disappeared in the middle of March in Liaodong Bay. Of course, the temporal change of SIA in this region almost followed the air temperature, as shown in Fig. 2.

Fig. 7(b) shows the temporal profile of daily SIA obtained from the MODIS Aqua sea ice product (MYD29), in which daily SIA coverage is very small as compared to the one from GOCI. Considering that the average of monthly sea ice coverage in the

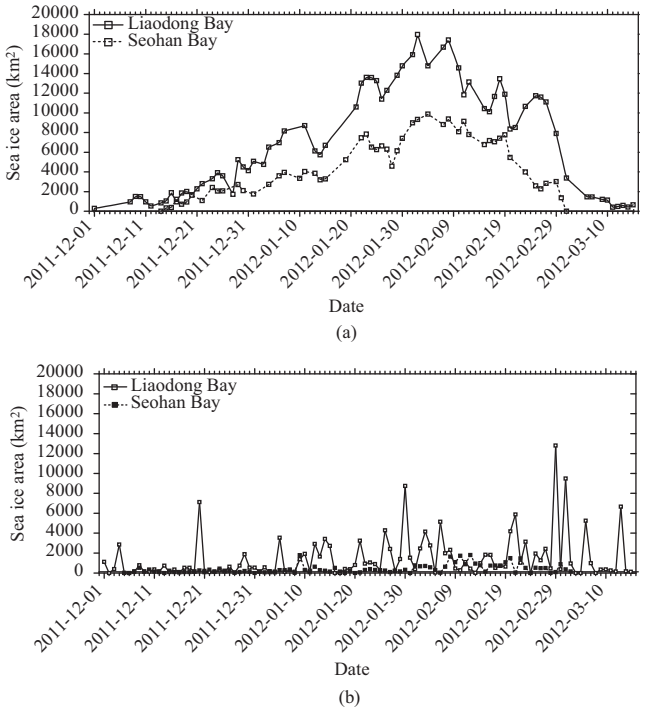

Fig. 7. Temporal changes of daily sea ice area (a) extracted from the GOCI images by the proposed spatial filtering method and from the MODIS sea ice product (b) in Liaodong and Seohan Bays during the ice period in the 2011-2012 winter.

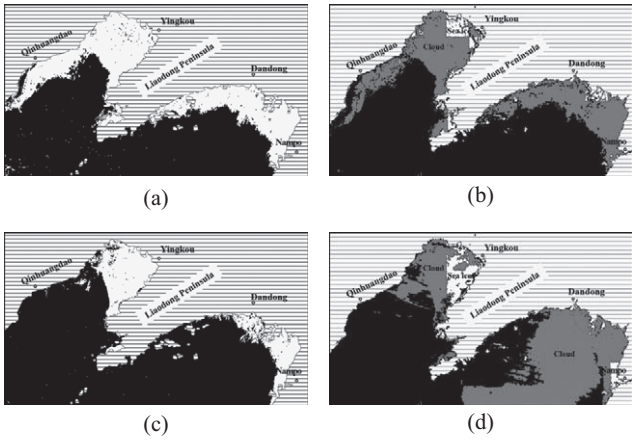

Fig. 8. Comparison of sea ice detection from GOCI images by the proposed filtering method (a, c) and from MODIS sea ice product (b, d). Both GOCI and MODIS Aqua images were obtained in clear sky condition. (a) and (b) were on February 4 while (c) and (d) were obtained on February 20, 2012.

Bohai Sea in January and February between 2002 and 2010 was larger than 10,000 km^2 (Shi and Wang, 2012b), the SIA in the MODIS product was very underestimated. Further, the temporal profile of SIA did not follow the typical bell-shaped seasonal pattern during the ice period, as seen in Fig. 7(a).

These erroneous SIA in the MODIS sea ice product could be explained by the difficulty to distinguish between sea ice and cloud. Fig. 8 compares the MODIS sea ice product with the SIA distribution extracted from GOCI in this study. While sea ice areas (Fig. 8(a)) were well detected from the GOCI images, they were mostly misclassified into cloud in MODIS product in this very clear day of February 4, 2012 (Fig. 8(b)). Sea ice coverages in Figs. 8(c) and 8(d) were obtained from GOCI and MODIS Aqua images on February 20, 2012. Again, most sea ice coverages were incorrectly detected as cloud in the MODIS product. In addition, Figs. 8(c) and 8(d) show the advantage of high temporal of GOCI to increase the chance of obtaining cloud-free images. The GOCI images were acquired at 10:00 in the morning under completely clear sky while the MODIS Aqua image was acquired at 14:00 and contaminated by large cloud coverage over Seohan Bay.

The MODIS sea ice detection method used multiple thresholds on band reflectance and NDSI (Hall et al., 1995) and did not have own cloud masking algorithm. Instead, MODIS cloud mask product (MYD35) was used to separate sea ice from cloud. MODIS cloud mask algorithm would be the most comprehensive since it used all the spectral characteristics of cloud in visible, NIR, shortwave infrared and thermal infrared bands (Ackerman et al., 1998). Although MODIS cloud mask algorithm was known to be highly accurate, it showed high confusion errors with sea ice in this region. MODIS sea ice and cloud mask algorithms were developed for global scale products and, therefore, might not reflect the local properties of sea ice in this region.

V. CONCLUSION

Sea ice monitoring in visible and NIR wavelength images is only applicable in cloud free regions. The Bohai and Yellow Seas are the lowest latitude area for seasonal sea ice formation in the world. Freezing air temperatures and strong wind from Siberian high pressure induce sea ice formation in the region from December to March. Sea ice in this region has caused several problems to sea transportation and harbor and offshore structures. This study demonstrated the potential of the unique GOCI geostationary satellite imagery for monitoring sea ice in this highly demanding and environmentally important sea area. GOCI provided relatively cloud-free daily images over sea ice for 91 days and 65 days during the 106 days and 80 days of the ice period in the 2011-2012 winter in Liaodong and Seohan Bays, respectively. GOCI even provided all eight hourly images with clear condition for 40 days in Liaodong Bay and for 31 days in Seohan Bay. GOCI is perhaps the first satellite imagery capable of tracking sea ice drift on an hourly basis.

We proposed a simple method to detect and extract SIA, utilizing the distinct spatial variation between sea ice and open water. Standard deviation filtering was very effective in delineating SIA from open water. In this study, we used Rayleigh corrected reflectance images. The atmospheric correction level did not affect the SIA detection results. Since the proposed method is based on the spatial variability between water and

ice, the type of pixel value does not affect very much. The sea ice detection results were not much different by the level of atmospheric correction, which would be advantage for reducing the data processing steps.

This study did not consider the ice thickness, which is a very important parameter in sea ice monitoring. Several studies have examined the relationship between the spectral reflectance or albedo of sea ice and its thickness (Grenfell, 1991; Su et al., 2012). The several types of sea ice in this region can be classified according to surface conditions, ice thickness, and sedimentation content within the ice. To develop a robust algorithm to assess sea ice thickness, the spectral characteristics of various ice types need to be refined. Although GOCI can provide large numbers of relatively cloud-free images for sea ice observation in this region, the cloud coverage over sea ice remains an obstacle in delineating the exact sea ice area. In this study, sea ice detections were only applied to the GOCI images obtained with clear sky condition. Further studies are needed to separate sea ice from cloud over the region. The spectral characteristics of clouds are similar to those of snow-covered and light-grey ices. Once cloud can be separated from sea ice, the temporal resolution of GOCI will be further improved.

ACKNOWLEDGEMENT

This research was a part of the project titled “Research for Applications of Geostationary Ocean Color Imager”, funded by the Ministry of Oceans and Fisheries, Korea.

REFERENCES

Ackerman, S. A., K. I. Strabala, W. P. Menzel, R. A. Frey, C. C. Moeller and L. E. Gumley (1998). Discriminating clear sky from clouds with MODIS. Journal of Geophysical Research 103(D24), 32141-32157.

Drüe, C. and G. Heinemann (2004). High-resolution maps of the sea-ice concentration from MODIS satellite data. Geophysical Research Letters 31, L20403.

Fensholt, R., A. Anyamba, S. Stisen, I. Sandholt, E. Pak and J. Small (2007). Comparisons of compositing period length for vegetation index data from polar-orbiting and geostationary satellites for the cloud-prone region of West Africa. Photogrammetric Engineering and Remote Sensing 73, 297-309.

Grenfell, T. C. (1991). A radiative transfer model for sea ice with vertical structure variations. Journal of Geophysical Research 96, 16991-17001.

Grenfell, T. C. and D. K. Perovich (1984). Spectral albedos of sea ice and incident solar irradiance in the southern Beaufort Sea. Journal of Geophysical Research 89, 3573-3580.

Hall, D. K., G. A. Riggs and V. V. Salomonson (1995). Development of methods for mapping global snow cover using moderate resolution imaging spectroradiometer data. Remote Sensing of Environment 54, 127-140.

Kang, G., P. Coste, H. Youn, F. Faure and S. Choi (2010). An in-orbit radiometric calibration method of the geostationary ocean color imager. IEEE Transactions on Geoscience and Remote Sensing 48, 4322-4328.

Lamquin, N., C. Mazeran, D. Doxaran, J. Ryu and Y. Park (2012). Assessment of GOCI radiometric products using MERIS, MODIS and field measurements. Ocean Science Journal 47, 287-311.

Lang, W., Q. Wu, X. Zhang, J. Meng, N. Wang and Y. Cao (2014). Sea ice drift tracking in the Bohai Sea using geostationary ocean color imagery. Journal of Applied Remote Sensing 8, 083650-083650.

Lee, K., S. Park, S. Kim, H. Lee and J. Shin (2012). Radiometric characteristics of Geostationary Ocean Color Imager (GOCI) for land applications. Korean Journal of Remote Sensing 28, 277-285.

Liu, J., R. Huang, Z. Jin, K. Wu and C. Sun (2000). Bohai sea ice monitoring using satellite images. Journal of Cold Regions Engineering 14, 93-100.

Ning, L., F. Xie, W. Gu, Y. Xu, S. Huang, S. Yuan, W. Cui and J. Levy (2009). Using remote sensing to estimate sea ice thickness in the Bohai Sea. China based on ice type. International Journal of Remote Sensing 30, 4539-4552.

Perovich, D., T. Grenfell, B. Light and P. Hobbs (2002). Seasonal evolution of the albedo of multiyear Arctic sea ice. Journal of Geophysical Research: Oceans (1978-2012) 107, SHE 20-1-SHE 20-13.

Riggs, G. A., D. K. Hall and S. A. Ackerman (1999). Sea ice extent and classification mapping with the Moderate Resolution Imaging Spectroradiometer Airborne Simulator. Remote Sensing of Environment 68, 152-163.

Ryu, J., H. Han, S. Cho, Y. Park and Y. Ahn (2012). Overview of geostationary ocean color imager (GOCI) and GOCI data processing system (GDPS). Ocean Science Journal 47, 223-233.

Scheuchl, B., D. Flett, R. Caves and I. Cumming (2004). Potential of RADARSAT-2 data for operational sea ice monitoring. Canadian Journal of Remote Sensing 30, 448-461.

Shi, W. and M. Wang (2012a). Sea ice properties in the Bohai Sea measured by MODIS-Aqua: 1. Satellite algorithm development. Journal of Marine Systems 95, 32-40.

Shi, W. and M. Wang (2012b). Sea ice properties in the Bohai Sea measured by MODIS-Aqua: 2. Study of sea ice seasonal and interannual variability. Journal of Marine Systems 95, 41-49.

Su, H., Y. Wang and J. Yang (2012). Monitoring the spatiotemporal evolution of sea ice in the Bohai Sea in the 2009-2010 winter combining MODIS and meteorological data. Estuaries and Coasts 35, 281-291.

Tschudi, M. A., J. A. Maslanik and D. K. Perovich (2008). Derivation of melt pond coverage on Arctic sea ice using MODIS observations. Remote Sensing of Environment 112, 2605-2614.

Yang, G. (2000). Bohai Sea ice conditions. Journal of Cold Regions Engineering 14, 54-67.

Yuan, S., W. Gu, Y. Xu, P. Wang, S. Huang, Z. Le and J. Cong (2012). The estimate of sea ice resources quantity in the Bohai Sea based on NOAA/AVHRR data. Acta Oceanologica Sinica 31, 33-40.

Yue, Q., D. Zhang, Y. Liu and B. Tong (2008). Failure modes analysis of ice-resistant compliant structures based on monitoring oil platforms in Bohai Gulf. The Ocean Engineering 26, 18-23.